

Supporting Information: Exciton transfer and localization in disordered Squaraine B polymers

David J. Fischermeier,* Arthur Turkin, Joschua Selby, Christoph Lambert, and Roland Mitrić

E-mail: david.fischermeier@gmail.com

Parameter development

Within NAMD, the VdW potential is calculated according to:

$$E_{VdW} = \epsilon_{ij} \left[\left(\frac{R_{ij}}{r_{ij}} \right)^{12} - 2 \left(\frac{R_{ij}}{r_{ij}} \right)^6 \right], \quad (1)$$

where ϵ_{ij} and R_{ij} constitute the average of the ϵ_i and ϵ_j or R_i and R_j atomic parameters respectively. r_{ij} denotes the distance between two atoms, i and j . The parameter development was done in a monte-carlo-esque fashion, in which a random change is perpetually performed on either ϵ , which is the depth of the VdW potential well and thus governs how strong the interaction binds, by ± 0.01 or R , which influences the position of the potential minimum, by ± 0.05 . A schematic of the process is shown in Fig. 1 and it consists of: (1)(Setup): Using initial VdW parameters obtained from similar molecules like indol and the other parameters obtained by FFTK, the helix was propagated in DCM and acetone, which leads to unfolding in both cases for this initial set of parameters. The total energies of the hexamer solvated in DCM ($E_{hex} + E_{solvation}$) are calculated along the unfolding trajectory for a set amount (e.g. 1000) of points. From the PES of the trajectory the total energy average of arbitrary

points close to the initial helical state and an average of arbitrary points at the final state are used to calculate ΔE_0 . A more in-depth explanation and reasoning for the setup is given in the S.I.. (2) A random step on the VdW parameters of the heavy ring system atoms is performed; (3) The total energies along the trajectory are recalculated based on the new parameters and ΔE is obtained as in (1); (4) If ΔE is lower than ΔE_0 , the changed parameters are accepted ΔE becomes ΔE_0 . Otherwise the changes are discarded. (5) repeat steps (2)-(4) for an arbitrary amount of steps. In this case after 100 steps, two MD simulations, i.e. the helix in acetone and DCM, with the new parameters were conducted for 10 ns to test the solvation behavior. If the solvation behavior was not yet satisfactory, the trajectory in DCM was then reinstated as the new pre-made trajectory as in (1).

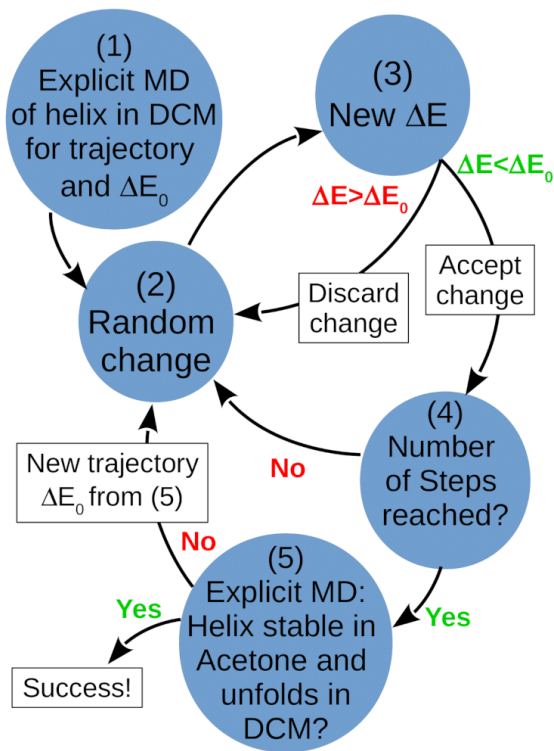


Figure 1: Schematic depiction of the VdW parametrization process.

Additionally we only included solvent molecules within 16 Å of the hexamer. This reduces the computational effort by several orders of magnitude, but introduces several problems as the trajectories no longer contain the same number of atoms (solvent), which means that calculating the enthalpic difference between the folded and unfolded has to be done by calculating the energy difference of the hexamer and its solvation energy only and thus neglecting the potential, kinetic energy of solvent molecules and solvent-solvent interactions.

$$\Delta E = E_{SQB,Initial} + E_{Solvation,Initial} - (E_{SQB,Final} + E_{Solvation,Final}) \quad (2)$$

Furthermore by changing the parameters, on which the PES is based on, the nature of the initial and final state shifts for every step and may or may not be actual stationary points. Thus we computed the initial and final state energy of an average of the lowest 5 structures within the first and last 10 structures respectively. These drastic shifts in the PES make it essential to swap the trajectory from which the energies are calculated with a new trajectory based on the most recent parameters often.

This process was aimed towards thermodynamic control by lowering the initial states energy in relation to the final state and fully ignores kinetic barriers. However, by lowering the energy of the initial state, one is also prone to increase the relative height of any barrier, which may result in a kinetically controlled reaction pathway.

For the purpose of our studies, this is mostly irrelevant however, as we are primarily interested in generating a stable helix in acetone and an unfolding helix in DCM, from which we wish to derive spectral data. Furthermore, since at the time, no quantitative, experimental data in regards to thermodynamic, entropic or kinetic behavior were present, we can not judge, which control mechanism is prevalent in reality.

MD energy profiles

The helical and linear hexamer were propagated in DCM and acetone for 10 ns.

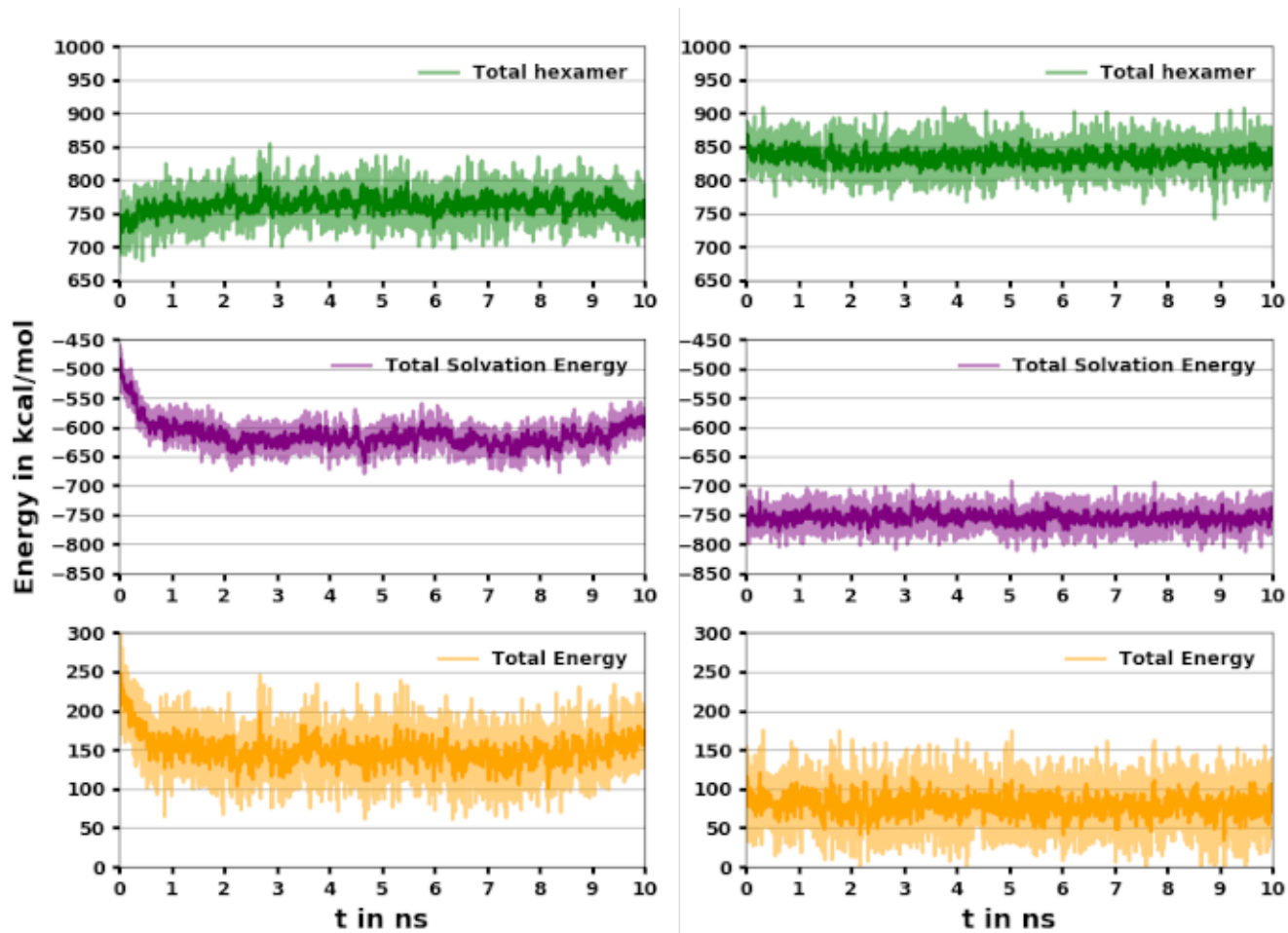


Figure 2: Energy profile of the stable helix in ACO on the left and the energy profile of the linear unfolded hexamer in ACO on the right. Within 1 ns the helix is equilibrated and stabilized. From the total energy, it can be seen, that the unfolded hexamer is thermodynamically favoured.

In acetone, as opted for by the parameter development process, the helix remains stable. As the helix becomes unfrozen at the start of the simulation and starts equilibration, the total energy of the hexamer increases slightly, while the solvation energy decreases resulting in a net decrease in total system energy. After 1 ns this process appears finished and the energies seem stable. The linear hexamer in acetone becomes more twisted and less ordered as expected. The energy profiles of this simulation do not change drastically over the course and reveal, that the unfolded hexamer in acetone should constitute the more stable species. In turn the helix in acetone appears to be kinetically trapped rather than thermodynamically stabilized.

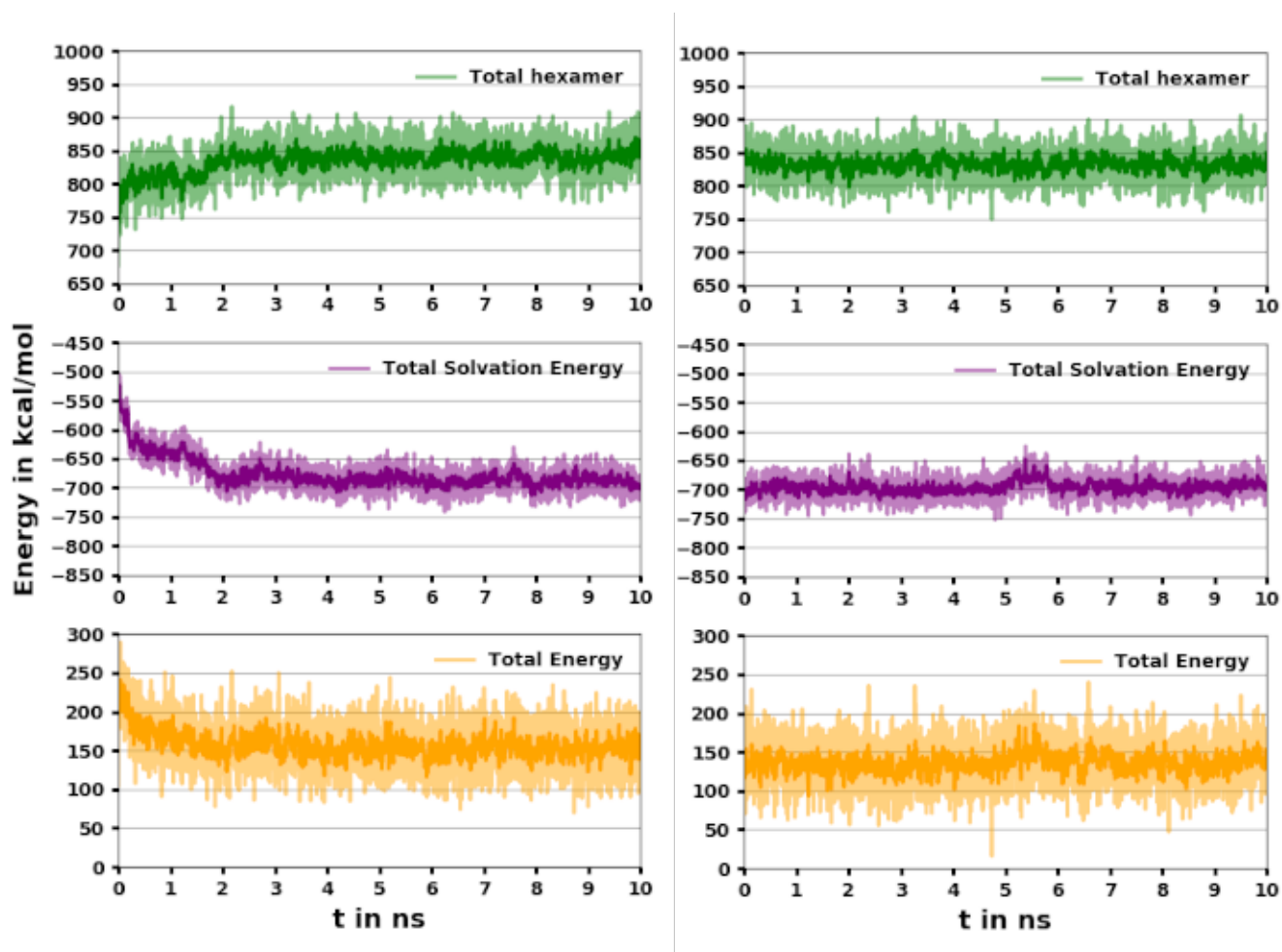


Figure 3: Energy profile of the helix unfolding in DCM on the left and the energy profile of the linear unfolded hexamer in DCM on the right. After 2 ns the unfolded helix converges with the linear hexamer's trajectory. No barrier for the unfolding process is observable.

In DCM the helix unfolds as we intended without any noticeable potential barrier within the first two nanoseconds, while the biggest change in solvation/total energy occurs during the first 500 ps. The energy converges nicely to the energy of the equilibrated linear hexamer easily within 10 ns, suggesting that the unfolding process is finished and the unfolded structure is equilibrated.

As mentioned earlier, the parametrization process was done by trying to lower the enthalpie of the unfolding process in DCM. In doing so, however, it appeared, that rather than achieving thermodynamic control, we were only able to establish a kinetic barrier, which prevents the helix from unfolding in acetone.

Stokes radius

To corroborate the validity of our MD generated helix structures in acetone further, we calculated the hydrodynamic/Stokes radius (R_0) using the SOMO software.¹⁻⁴ We employed the AtoB grid based model with cubelettes of 0.5 nm side length. The residue parameters were constructed by the software from the provided, averaged, default parameters. This may not be fully correct, but the visualized bead models shown in Fig. 4 show a very accurate volumetric representation of the helix. The calculations were conducted for a superposition of the aligned structures of the 10ns ensemble in acetone, which was also used for all other calculations. R_0 was calculated once with and without the aliphatic tails. As those tails are much less rigid compared to the core conjugated helix system their inclusion might yield unrealistically high values for R_0 , although their influence on the bulk of the molecule should not be fully neglected. Both calculations should provide a good upper and lower bound for R_0 .

DOSY NMR measurements were performed in acetone- d_6 and CD_2Cl_2 as shown in Fig. 6. R_0 of the hexamer was calculated from the corresponding diffusion coefficients D of the Stokes-Einstein equation at 293 K:

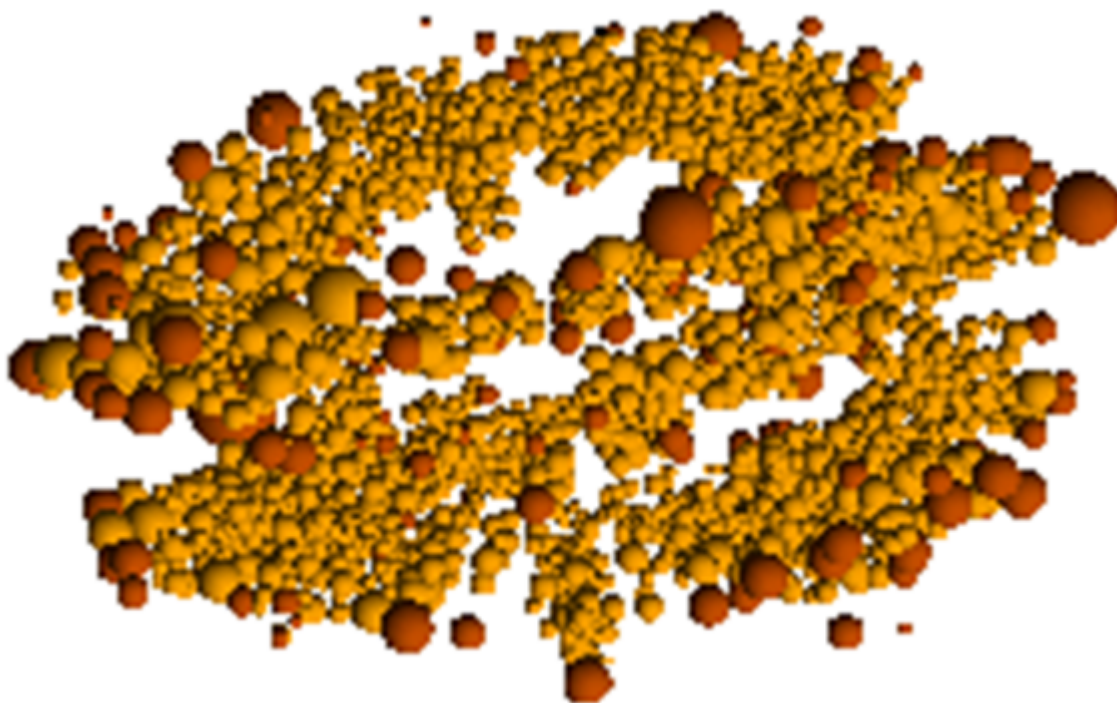


Figure 4: AtoB bead model with a cubelett side length of 0.5 Å of the 10 ns ensembles without its aliphatic tails.

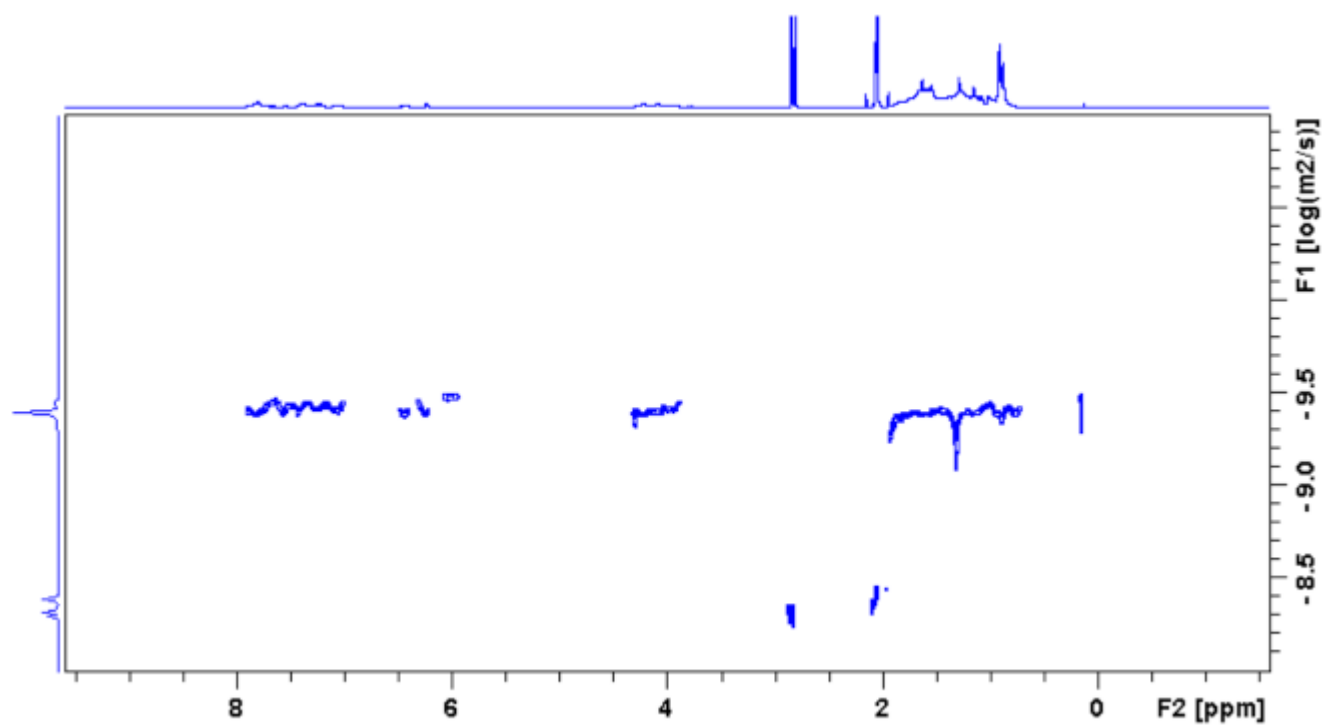


Figure 5: DOSY NMR spectrum of the SQB hexamer in acetone-*d*₆. Here, R_0 is 1.69 nm.⁵

$$D = \frac{k_B T}{6\pi\eta R_0} \quad (3)$$

where k_B is the Boltzmann constant, T is the temperature, and η is the viscosity of the solvent ($\eta_{\text{acetone}} = 3.20 \times 10^{-4} \text{ Ns m}^{-2}$). The sample concentration of each measurement is approx. 10^6 M , thus not adjusted to the number of repeating units. For the evaluation of the data the TopSpin Software (v.3.2) by Bruker GmbH was used. Therefore the data were handled according to the TopSpin documentation: the squaraine peaks were integrated and the exported data fitted with the function type "vargard". The resulting diffusion constants were averaged and further processed via the Stokes-Einstein equation. One needs to keep in mind that the Stokes-Einstein equation is suitable only for spherical molecules and the helix resembles rather a cylinder. And while there are numerous equations for different geometries to calculate R_0 , the Stokes-Einstein equation will suffice in the relative context of this investigation.

Our calculations show R_0 values of 1.82 nm and 1.60 nm with and without tails respectively, which corresponds very nicely to the experimentally derived 1.79 nm. It should again be noted, that we used a superposition of multiple geometrically aligned ensemble structures, which naturally inflates the value and it indicates that the modelled helix is most likely too compact.

Circular dichroism spectroscopy

Aside from UV-Vis absorption spectra we also calculated the CD spectra for the helix in acetone to provide further evidence pointing toward a helical structure. Unfortunately the lc-TDDFTB software used is incapable of calculating CD spectra. Utilizing regular TD-DFT for a whole ensemble would be tremendously expensive in terms of computational resources and thus, we constructed an multiple "ideal" helix structures from an optimized monomer with differing dihedral angles and sheet distances between 5 and 7 Å, which was the range we

observed in our MD simulations. The calculations were carried out with Gaussian16⁶ on a CAM-B3LYP⁷/def2-SVP^{8,9} level, which was the basis for the lc-TDDFTB parametrization. An ϵ of 20.493 to simulate acetone as a polarizable continuous medium (PCM) was used as well. As SQB is achiral, the direction in which the helix is folded (clockwise or counterclockwise) is random as well. In order to guide the helix folding experimentally, chiral parts were introduced into the aliphatic tails resulting in CD activity.

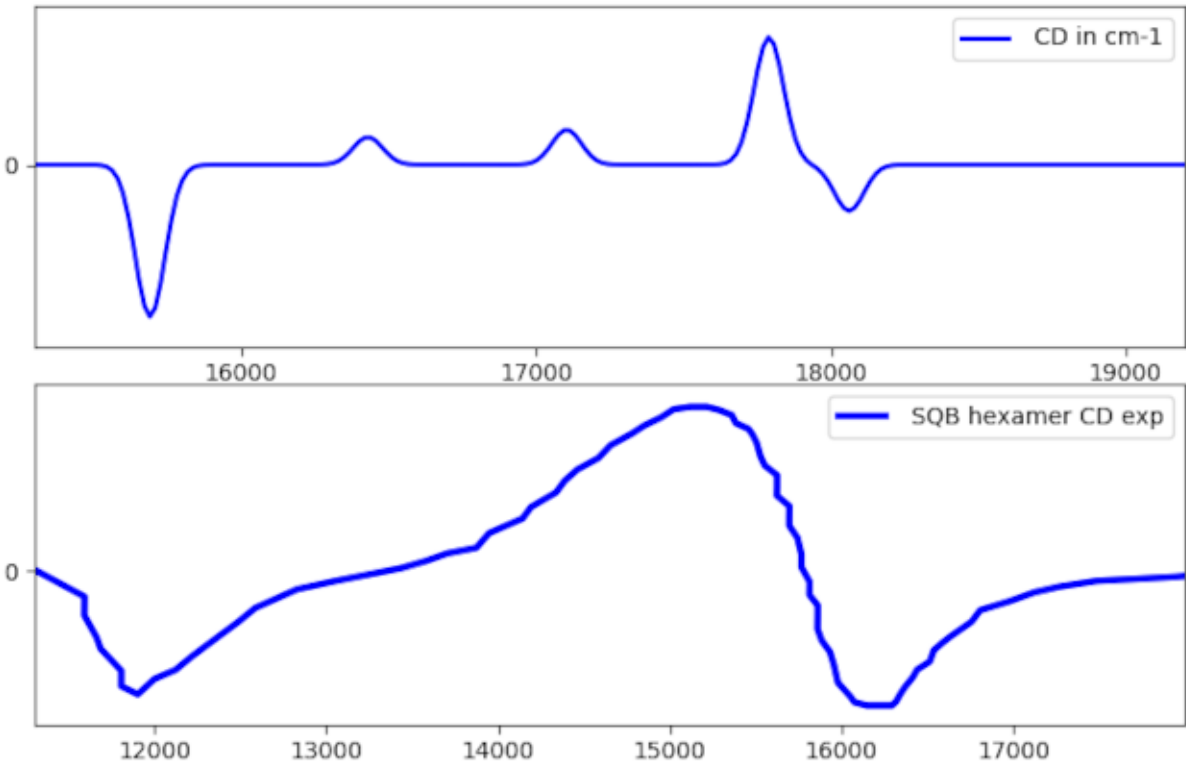


Figure 6: Comparison of CD spectra from TD-DFT (top) and experimental measurements for a mixture of longer polymer chains (average length 36.1 units) (bottom).

The TD-DFT calculation overestimates the absorption energy by roughly 3000 cm^{-1} and underestimates the signal's splitting. Qualitatively the resemblance of both spectra is fairly good, although the final peak in the theoretical spectrum at 18000 cm^{-1} does lack in intensity compared to the experiment. However, since CD spectra are by their nature very sensitive to the relative orientation between electric and magnetic transition dipole moments, a good

agreement in spectral shape likely suggests a good agreement in the studied structures.

Exciton model calculations on the localization of the hexamer

Using the exciton model we have calculated the absorption spectrum for the helix in acetone after 10ns, which was also used for the lc-TDDFTB calculations. As with the exciton spectra conducted in DCM, we used the optimized SQB monomer’s transition energies (17158 cm^{-1}) and transition charges derived from GAUSSIAN09¹⁰ with CAM-B3LYP⁷ on the def2-SVP^{8,9} and MultiWFN 3.5.^{11,12}

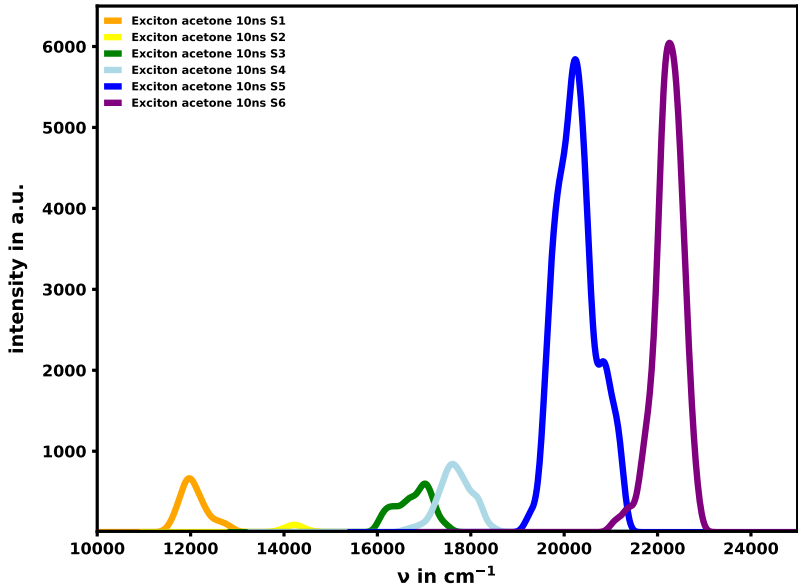


Figure 7: Absorption spectrum of the 100 structure ensemble of the helix in acetone after 10 ns of MD simulation. The signals were broadened with a FWHM of 120 cm^{-1} .

We see a clear prominence of the blueshifted signals from the S_5 and S_6 transitions. The splitting of the signals is much more pronounced than we saw for the lc-TDDFTB or experimental spectra, but qualitatively they align well. We also observe very weak bands in

the energetically lower regions of the S_1 and S_2 states, which were more pronounced in the experiment and lc-TDDFTB calculations.

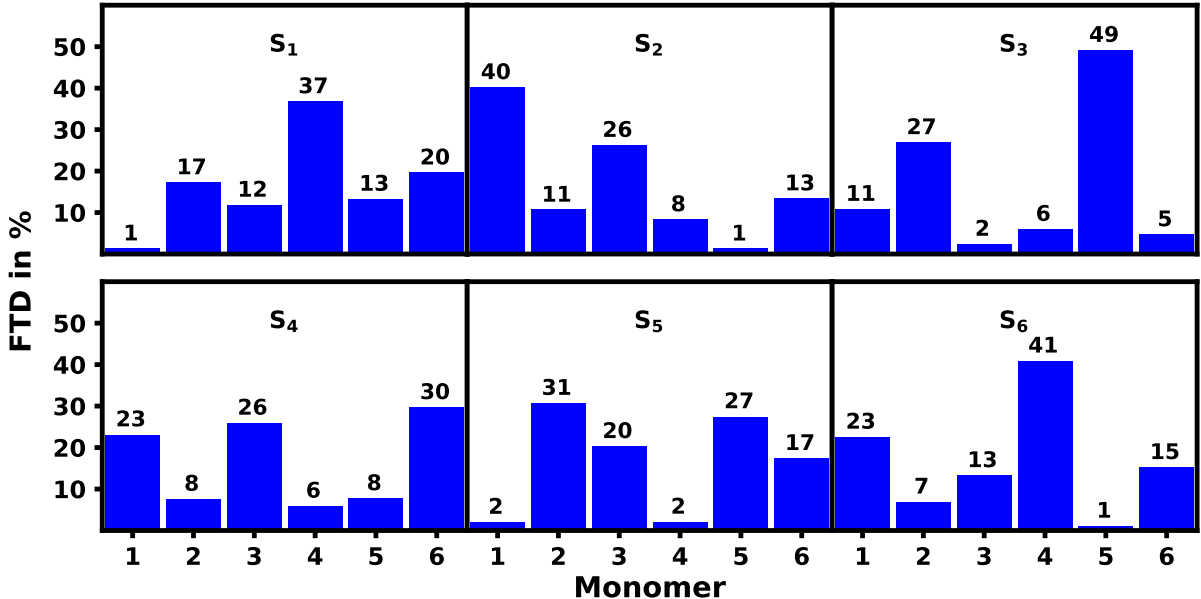


Figure 8: FTD per monomer for the helix in acetone at 10 ns calculated with the exciton model.

Analyzing the fraction of the transition densities we see a slightly different picture than we observed in the lc-TDDFTB spectra. The S_1 transition is now mostly localized on M4 and has the lowest FTD on M1, which held the highest contribution in the lc-TDDFTB calculations. Furthermore, the S_6 transition is now mostly localized on M1&M4, which is in full opposition to the lc-TDDFTB results, where the S_1 and S_6 transitions localized on different sites, but occur on the same site, M4, in the exciton picture. This is not surprising as the monomer pair contributing to the highest (and often brightest) transition also contributes to the lowest (and often darkest) transition, since they "split" the monomer's signal the furthest. The exciton model does not include any orbital interaction, which are assumed to be paramount in such a densely stacked and covalently bonded/conjugated π -system like a helix. These interactions might well stabilize the S_1 transition on M1 and likewise destabilize the S_6 transition on M4. It does, however, appear curious, that the most remote monomers

M1&M4 would form the strongest H-aggregate in the helix. We would expect the two closest monomers to form the strongest H-aggregate and localize the S_6 transition.

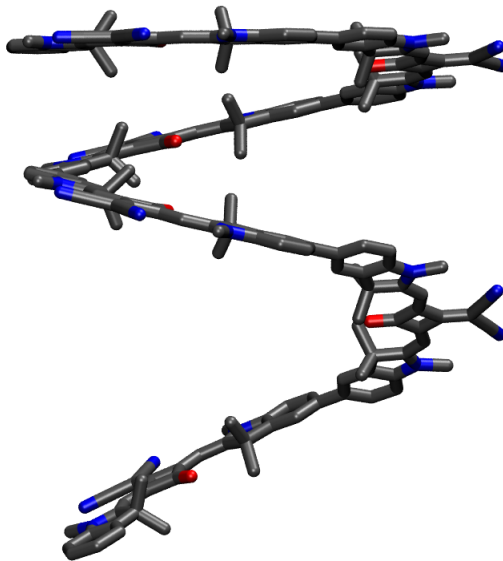


Figure 9: Structure of a widening hexamer helix.

To test the reliance of the exciton model, we have constructed a model helix, which widens its pitch with each monomer as seen in Fig 9.

The localization pattern shown in Fig 10 reveals the expected behavior, where the closest monomers M1&M4 localize the both the S_1 and S_6 transition in the model system. We have to attribute this difference in behavior between the ideal widening helix and the structures taken from the MD simulations to an interplay of multiple geometric factors arising from the specific orientations between the monomers.

There are also some interesting trends when examining the S_2 and S_5 states (Fig 11 for the exciton spectrum of the 10ns ensemble of the helix, which fully reproduce the lc-TDDFTB results, we saw for the S_1 and S_6 transitions. When combining the S_5 & S_6 transition density, we still find that M4 exhibits the highest FTD, but M1 exhibits the lowest, where both exhibit the highest FTD for the combined S_1 & S_2 transitions. So while the reproduction of the lc-TDDFTB calculations is far from perfect, we still see the overall trend of the low

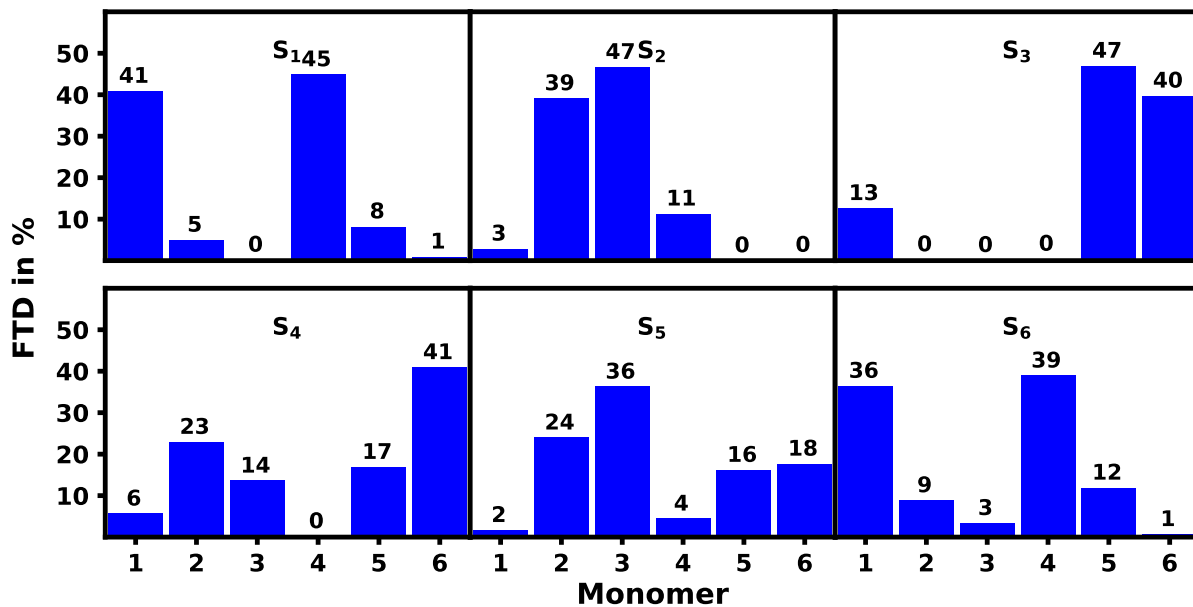


Figure 10: FTD distribution for the widening hexamer helix model system.

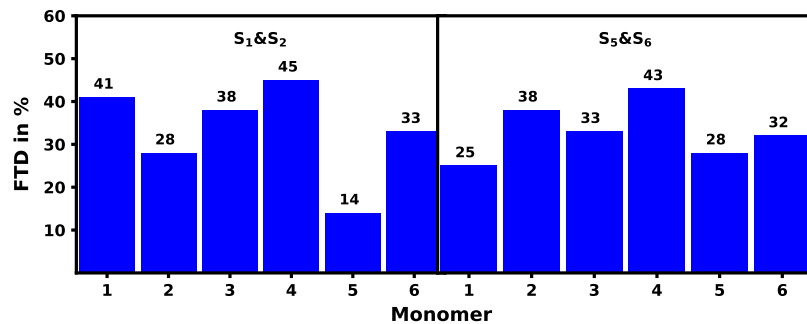


Figure 11: Combined FTD per monomer for the helix in acetone at 10 ns calculated with lc-TDDFTB for the S₁&S₂ state as well as S₅&S₆.

energy transitions occurring more on the M1&M4 monomers reproduced, while the monomer pair with the highest FTD contribution for the higher energy transitions S_5 & S_6 is found to be M3&M6, which also exhibited a high FTD for the lc-TDDFTB calculations. In summary, the

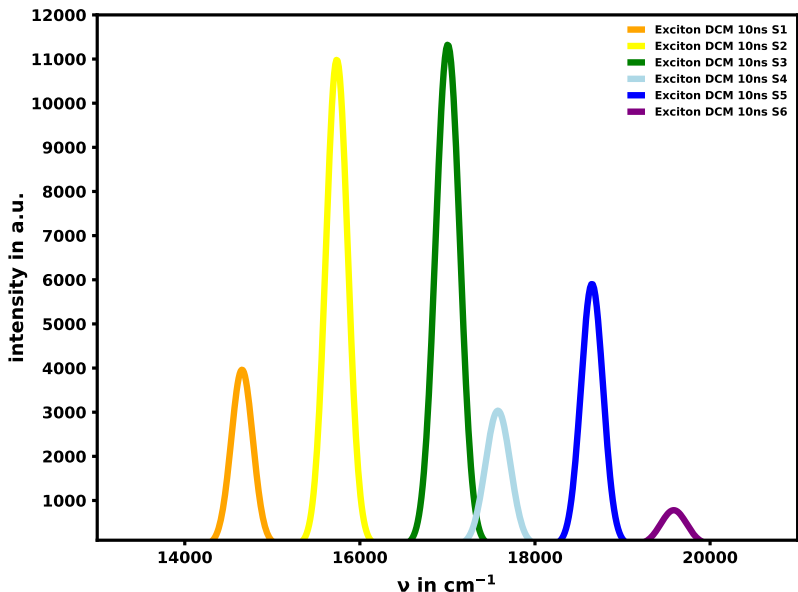


Figure 12: Absorption spectrum of the 100 structure ensemble of the unfolded helix in DCM after 10 ns of MD simulation. The signals were broadened with a FWHM of 120 cm^{-1} .

exciton model does give results, which overall are in good agreement with the lc-TDDFTB results, but differ in some details. The clearly show the prominence of H-aggregation in the helix and J-aggregation of the unfolded helix, which is also seen in the coupling terms shown in Fig. 13 and Fig. 14. Most importantly, it does reproduce the experimental finding, where the S_1 and S_6 exciton was transiently found on the same site, which was one discrepancy between the experiments and lc-TDDFTB, which was discussed in the main text. So both methods seem to be complement each other very well in this instance, while the exciton model failed to reproduce the exciton localization in the unfolded system in DCM as discussed, but produced good agreement in terms of the absorption spectrum with a red-shifted main absorption signal and pronounced shoulder in the blue-shifted bands as the experimental

and lc-TDDFT spectra show (Fig. 12).

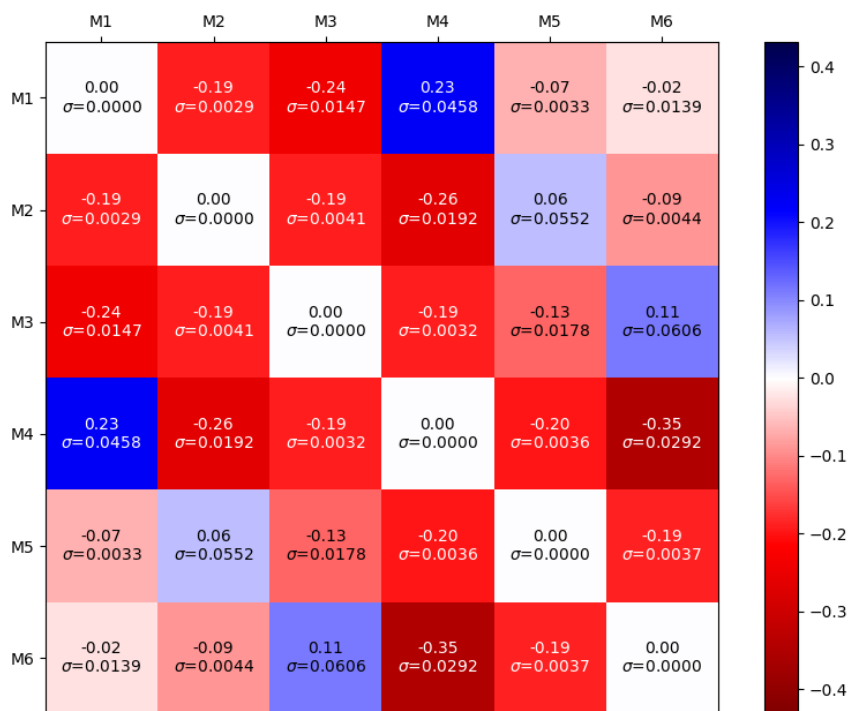


Figure 13: Average Coulomb couplings and their standard deviations for the helix in acetone at 10ns.

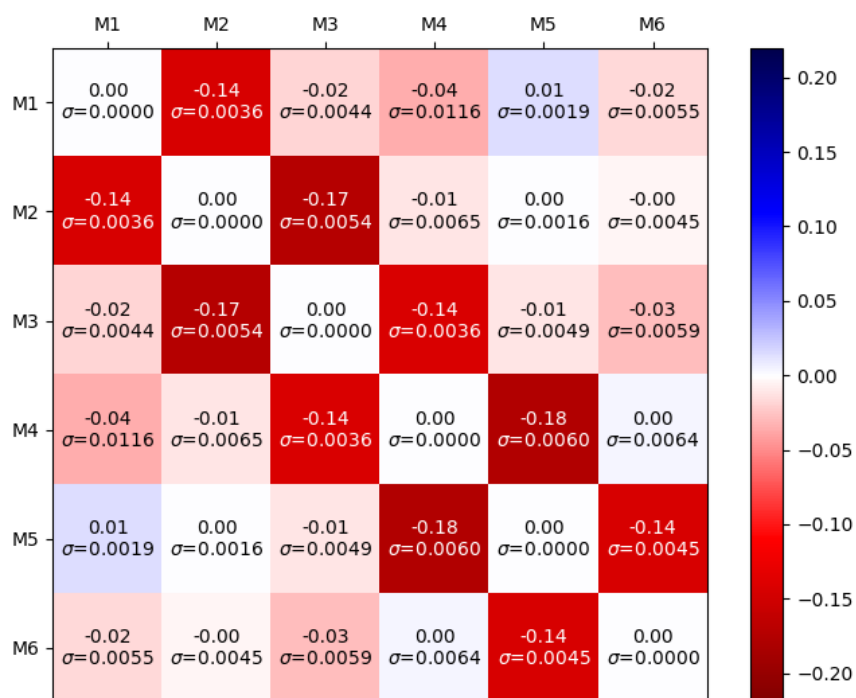


Figure 14: Average Coulomb couplings and their standard deviations for the unfolded helix in DCM at 10ns.

Complementary localization data for the SQB hexamer

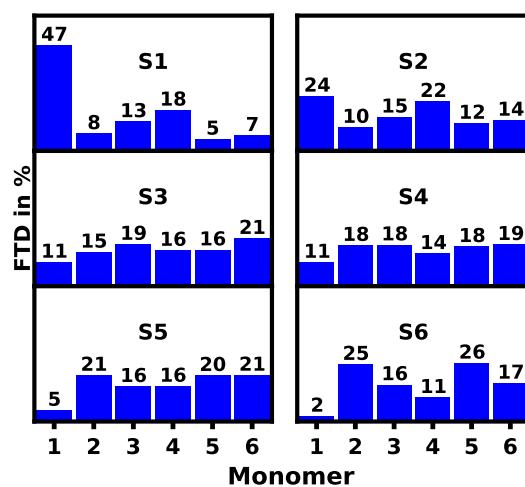


Figure 15: FTD per monomer for the helix in acetone at 10 ns calculated with lc-TDDFTB.

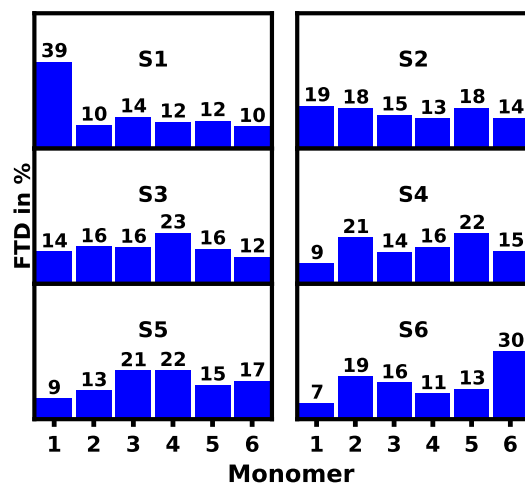


Figure 16: FTD per monomer for the helix in DCM at 10 ns.

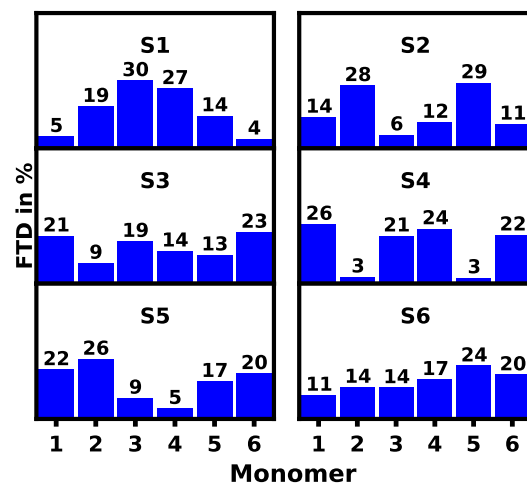


Figure 17: FTD per monomer for the reconstructed ensemble of the helix in DCM at 10 ns.

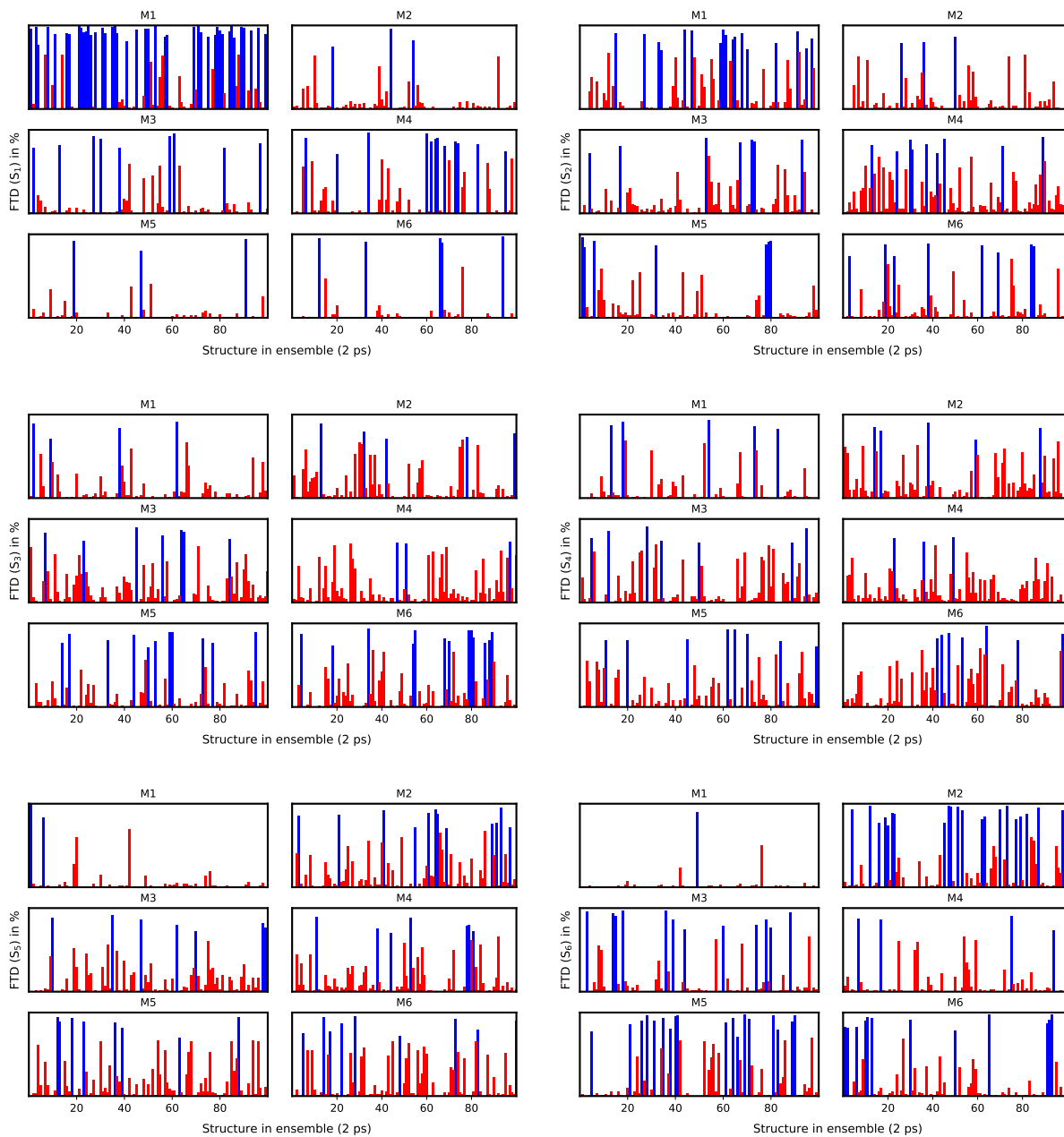


Figure 18: FTD per ensemble structure for the helix in acetone at 10 ns.

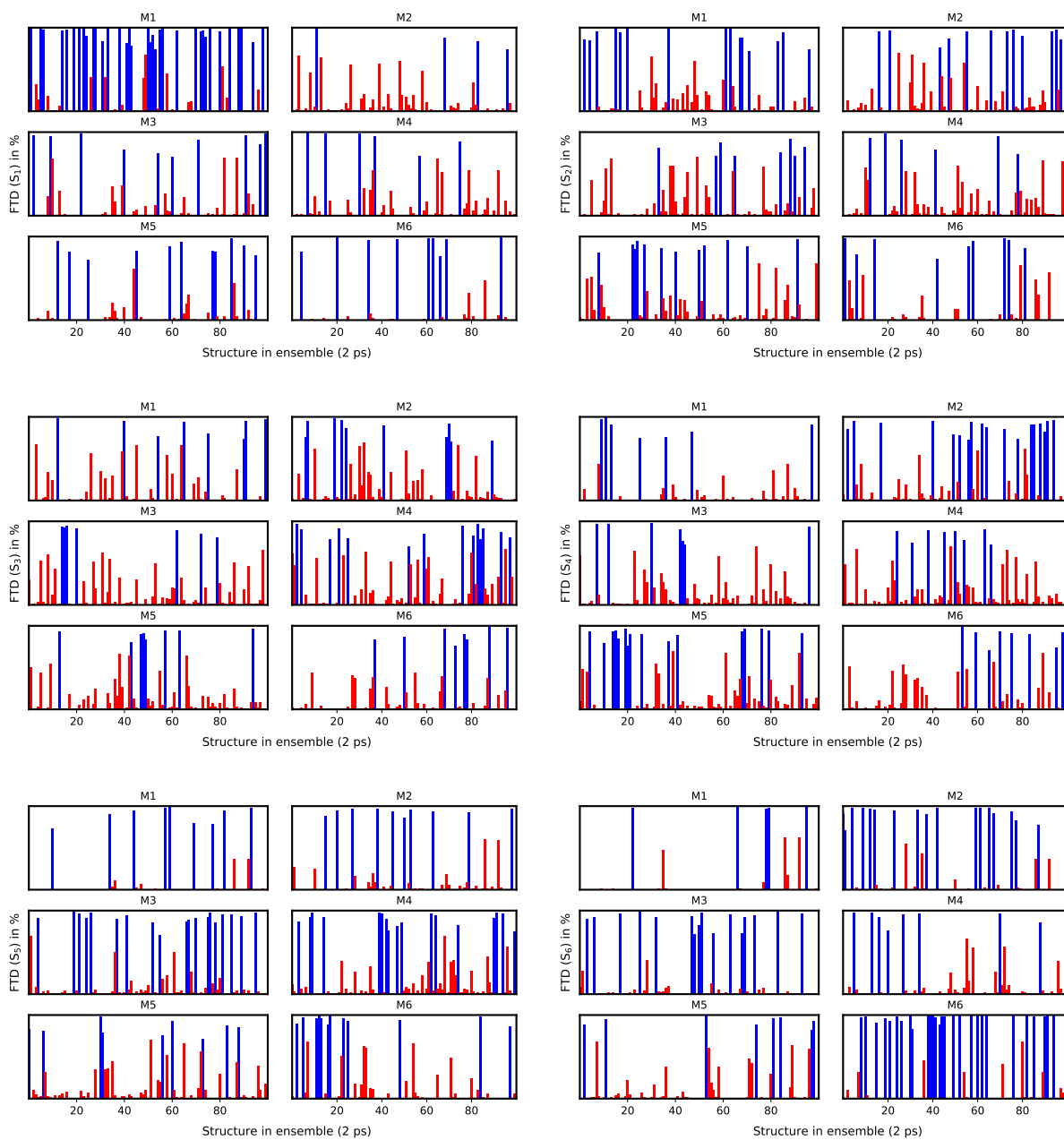


Figure 19: FTD per ensemble structure for the helix in DCM at 10 ns. The blue bars indicate a strong localization with over 70% of FTD being localized on a monomer, while the red bars indicate lower than 70% localization.

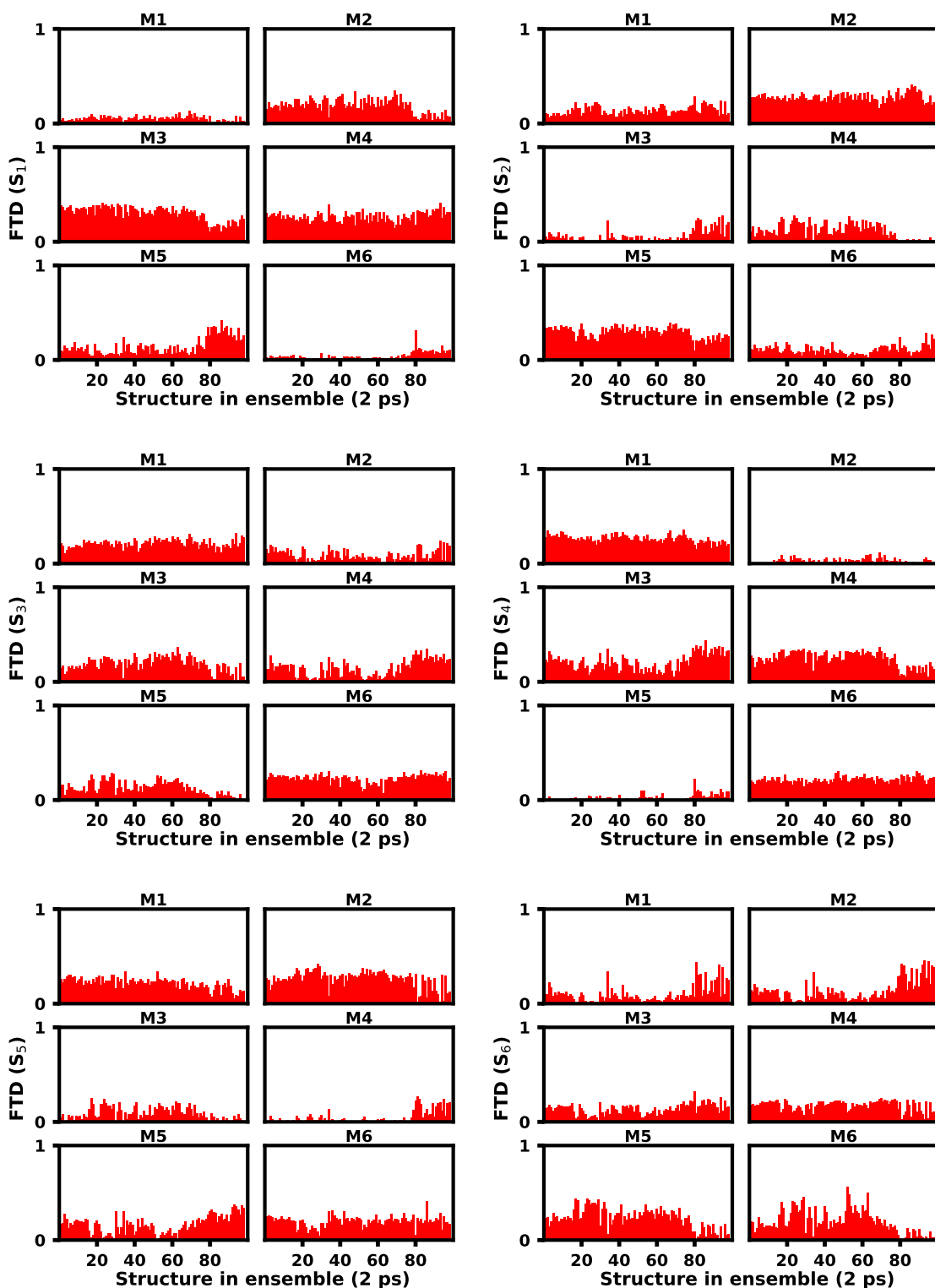


Figure 20: FTD per ensemble structure in the reconstructed ensemble for the helix in DCM at 10 ns. The blue bars indicate a strong localization with over 70% of FTD being localized on a monomer, while the red bars indicate lower than 70% localization.

References

- (1) Byron, O. Construction of hydrodynamic bead models from high-resolution X-ray crystallographic or nuclear magnetic resonance data. *Biophysical Journal* **1997**, *72*, 408–415.
- (2) Brookes, E.; Demeler, B.; Rosano, C.; Rocco, M. The implementation of SOMO (Solution MOdeller) in the UltraScan analytical ultracentrifugation data analysis suite: enhanced capabilities allow the reliable hydrodynamic modeling of virtually any kind of biomacromolecule. *European Biophysics Journal* **2010**, *39*, 423–435.
- (3) Zuk, P. J.; Cichocki, B.; Szymczak, P. GRPY: An Accurate Bead Method for Calculation of Hydrodynamic Properties of Rigid Biomacromolecules. *Biophysical Journal* **2018**, *115*, 782–800.
- (4) Rocco, M.; Brookes, E.; Byron, O. In *Encyclopedia of Biophysics*; Roberts, G., Watts, A., Eds.; Springer Berlin Heidelberg: Berlin, Heidelberg, 2020; pp 1–11.
- (5) Turkin, A.; Holzapfel, M.; Agarwal, M.; Fischermeier, D.; Mitric, R.; Schweins, R.; Gröhn, F.; Lambert, C. Solvent Induced Helix Folding of Defined Indolenine Squaraine Oligomers. *Chemistry – A European Journal* **2021**, *27*, 8380–8389.
- (6) Frisch, M. J. et al. Gaussian~16 Revision C.01. 2016.
- (7) Yanai, T.; Tew, D. P.; Handy, N. C. A new hybrid exchange–correlation functional using the Coulomb-attenuating method (CAM-B3LYP). *Chemical Physics Letters* **2004**, *393*, 51–57.
- (8) Weigend, F.; Ahlrichs, R. Balanced basis sets of split valence, triple zeta valence and quadruple zeta valence quality for H to Rn: Design and assessment of accuracy. *Physical Chemistry Chemical Physics* **2005**, *7*, 3297.

- (9) Weigend, F. Accurate Coulomb-fitting basis sets for H to Rn. *Physical Chemistry Chemical Physics* **2006**, *8*, 1057.
- (10) Frisch, M. J. et al. *Gaussian09 Revision E.01*.
- (11) Lu, T.; Chen, F. Calculation of Molecular Orbital Composition. *Acta Chimica Sinica -Chinese Edition-* **2011**, *69*, 2393.
- (12) Lu, T.; Chen, F. Multiwfn: a multifunctional wavefunction analyzer. *Journal of computational chemistry* **2012**, *33*, 580–592.